

Photon Upconversion in Hetero-nanostructured Photoanodes for Enhanced Near-Infrared Light Harvesting

Liap Tat Su, Siva Krishna Karuturi, Jingshan Luo, Lijun Liu, Xinfeng Liu, Jun Guo, Tze Chien Sum, Renren Deng, Hong Jin Fan, Xiaogang Liu,* and Alfred Ling Yoong Tok*

Photon upconversion of sunlight by lanthanide-doped materials is an emerging concept to improve solar energy conversion efficiency.^[1–3] For conventional solar cells, one of the major energy loss mechanisms is the transmission of sub-bandgap photons. The use of upconversion materials provides a solution to the transmission loss by converting two sub-bandgap photons into one above-bandgap photon. Indeed, upconversion particles have been coupled to a wide range of solar cells including crystalline Si,^[4] amorphous Si thin-film,^[5] organic,^[2a] and dye-sensitized solar cells.^[6] Despite the emerging prospects, the integration of upconversion particles with existing systems has not resulted in much improved solar cell performance. One major limiting factor to the low conversion efficiency is the spatial incorporation of upconversion materials in solar cells.^[1,2b] Generally, upconversion materials are added as an ex-situ planar layer on top of a reflector. This layer can absorb the near-infrared part of the solar spectrum transmitted through the bifacial solar cell, and then emit visible photons which are then directed back to the rear surface of the solar cell through an internal reflector. However, only a small fraction of the upconverted light is captured by the solar cell because of energy losses due to internal scattering and absorption.

To solve the issue, an alternative solution where an in-situ placement of upconversion particles in solar cell was reported recently.^[6a] The upconversion particles were mixed with titanium oxide particles to form a composite material, which was subsequently used as part of a working electrode for dye-sensitized solar cells. This in-situ architecture is a better strategy as the close contact between the upconversion particles and photon-absorbing dye ensures immediate absorption

of the emitted light and reduces transmission loss. However, the energy efficiency of the dye-sensitized solar cell with the composite layer was found to be almost the same as that for the conventional dye-sensitized solar cell. This is attributed to the impedance to the flow of electrons caused by the presence of upconversion particles, leading to the charge carrier losses. In addition, direct irradiation of upconversion particles in the form of the proposed in-situ architecture has proven difficult.

Herein, we report a rational design and fabrication of interconnected porous network of three-dimensional hetero-nanostructured photoanodes for enhanced near-infrared light harvesting. As shown in **Scheme 1**, the photoelectrode constitutes a titanium oxide (TiO₂) inverse opal, which optimally conducts electrons with minimal carrier losses due to its continuous electron conducting pathways. The three-dimensional hierarchical porous network of the inverse opal not only provides a large interfacial surface area for efficient loading of upconversion nanoparticles and quantum dot sensitizers, but also allows an excellent interaction between the electrolyte and quantum dots. In addition, the inverse opal is known to improve the light-matter interaction because of the strong light scattering and increased path length travelled by the light in the electrode.^[7–9] By using the as-fabricated photoanode, we successfully demonstrated hydrogen generation via a photoelectrochemical process driven by near-infrared irradiation.

In a typical experiment, monodispersed polystyrene microspheres of ~510 nm in diameter were self-assembled onto fluorine-doped tin oxide substrates to form sacrificial opal templates by an evaporation-induced convective deposition method (**Figure 1a**).^[10] These polystyrene opal photonic crystals form a face-centered cubic lattice structure with a hierarchical long-range order. Subsequently, TiO₂ was then infiltrated through the opal templates by an atomic layer deposition method.^[11] As demonstrated in our previous works,^[7–9,12] a near-theoretical filling fraction can be achieved through the conformal coating process. The TiO₂-infiltrated opal templates were then subjected to pyrolysis at 450 °C to thermally remove the polystyrene spheres, leaving behind the TiO₂ inverse opal photonic crystals with an anatase phase and 6 μm in film thickness (**Figure 1b**).

The photonic crystals show wide pore interconnectivity and hierarchically ordered periodicity. These are important attributes for the subsequent infiltration of upconversion nanoparticles, sensitization of quantum dots, and penetration of electrolyte throughout the entire photoanode. In our proof-of-concept experiment, upconversion nanoparticles composed of NaYF₄:Yb³⁺/Er³⁺@NaYF₄ core-shell nanoparticles (~30 nm) were used (**Figure S1**, Supporting Information). The core-shell nanoparticles, as previously reported, exhibit efficient upconversion

Dr. L. T. Su,^[†] S. K. Karuturi,^[†] Dr. L. Liu, J. Guo, Prof. A. I. Y. Tok
School of Materials Science and Engineering
Nanyang Technological University, Singapore 639798
E-mail: MIYTok@ntu.edu.sg

J. S. Luo, Dr. X. Liu, Prof. T. C. Sum, Prof. H. J. Fan
Division of Physics and Applied Physics
Nanyang Technological University, Singapore 639798

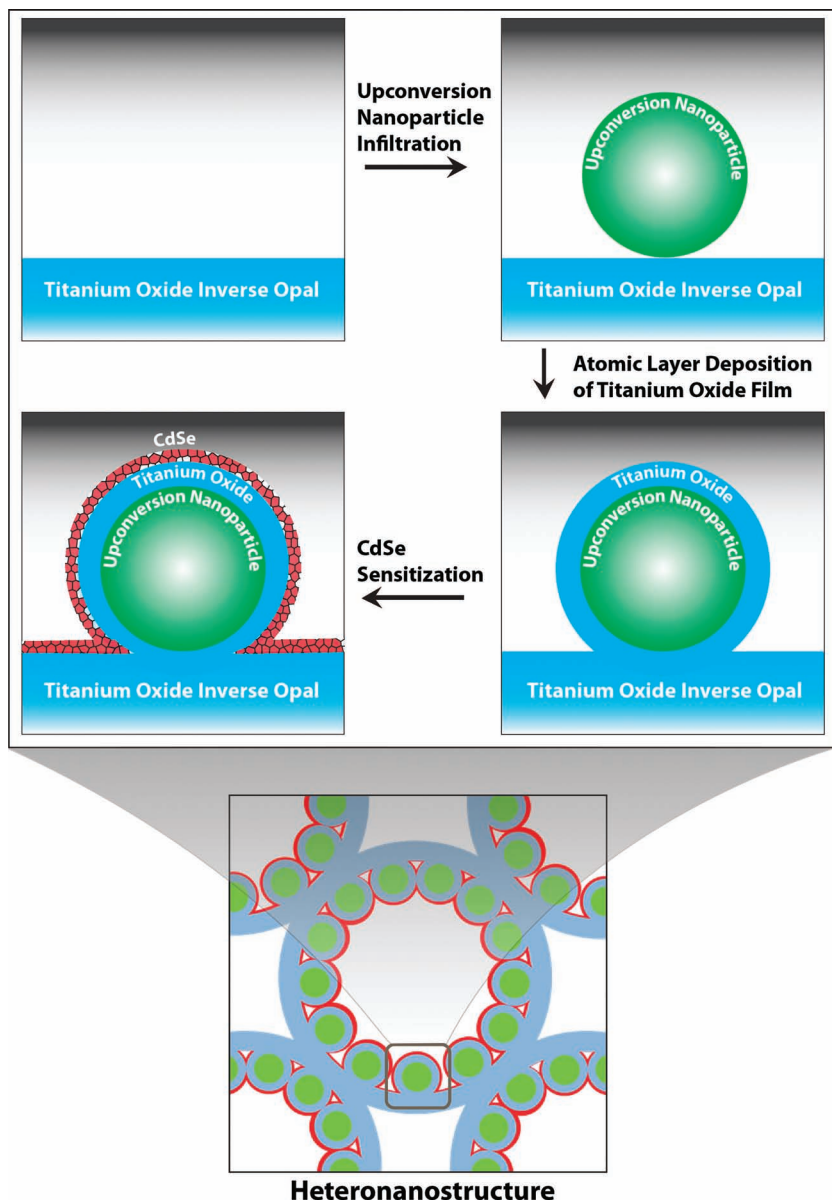
R. Deng, Prof. X. Liu
Department of Chemistry
National University of Singapore, Singapore 117543
E-mail: chmlx@nus.edu.sg

Prof. X. Liu
Institute of Materials Research and Engineering
3 Research Link, Singapore 117602

^[†]These authors contributed equally to this work.



DOI: 10.1002/adma.201204353



Scheme 1. A schematic representation showing the fabrication process for a porous hetero-nanostructured photoanode.

emission due to the surface coating.^[1h,13] The incorporation of these nanoparticles into the hetero-nanostructured photoanode as a conformal layer enables the photoresponse investigation of the photoelectrochemical cells. The infiltration of the nanoparticles was made possible through the capillary effect of the porous network under high vacuum, which allowed homogeneous distribution of the nanoparticles on the surface of the inverse opal (Figure 1c, d).

Prior to the final coating of quantum dots sensitizers, a thin layer of TiO₂ was deposited onto the nanoparticles by an atomic layer deposition technique (Figure 1e, f). This coating ensures the continuation of TiO₂ matrix is made available for the interfacial contact with the subsequent quantum dots attachment, as it is pivotal in the process of keeping electron injection from

quantum dots to TiO₂. After the deposition, an annealing step was required to crystallize TiO₂ but the temperature must be controlled to prevent the transformation of upconversion nanoparticles from hexagonal to cubic phase. This is an important step as the emission intensity of the hexagonal-phase NaYF₄ is about 10 times stronger than that of its cubic counterpart.^[14] Through X-ray diffraction measurements, we found that 300 °C is the optimal temperature to maintain hexagonal phase of the nanoparticles while crystallizing TiO₂ as the anatase phase (Figure S2, Supporting Information). It is noted that the nanoparticles adsorbed on the inverse opal can further increase the effective contact surface areas to achieve higher loading of quantum dots, which in turn results in higher interfacial contact area for the quantum dots with electrolytes and thus higher photocurrent.

To form a working electrode, we used CdSe quantum dots sensitizer to coat the hetero-nanostructures via a modified successive ionic layer adsorption and reaction route.^[15] The as-prepared photoanode has maintained the ordered periodicity of the photonic crystals with surfaces uniformly covered by quantum dots (Figure S3, Supporting Information). The three-dimensional periodicity arrangement has also been validated by specular reflectance measurements (Figure S4, Supporting Information). This measurement is possible due to the highly periodic arrangement of spherical pores in the photonic crystal, which prohibits the propagation of light through the structure. This effect is known as photonic bandgaps corresponding to the reflectance peaks obtained in the specular reflectance spectrum. In the case of TiO₂ inverse opal, the wavelength of reflectance peak is centered at 897 nm. After the infiltration of upconversion nanoparticles, the peak shifts to 958 nm. For the final coating of the quantum dots on

the photoanode, the photonic stopband is centered at 1146 nm. Throughout various stages of materials infiltration, the reflectance peaks are sharp and symmetrical and the corresponding intensities remain high. This indicates that a uniform coverage of upconversion nanoparticles and quantum dots has been achieved on the inverse opal and the structure integrity of the TiO₂ inverse opal is robust even after a series of material infiltration and annealing steps. There is no anomaly observed for aggregation of nanoparticles or pore clogging.

When the photoanode is excited by near-infrared light, the upconversion nanoparticles emits green and red light, corresponding to ²H_{11/2}, ⁴S_{3/2} → ⁴I_{15/2} and ⁴F_{9/2} → ⁴I_{15/2} transitions of Er³⁺, respectively (Figure S5, Supporting Information).^[16] The emitted visible light is readily absorbed by the quantum

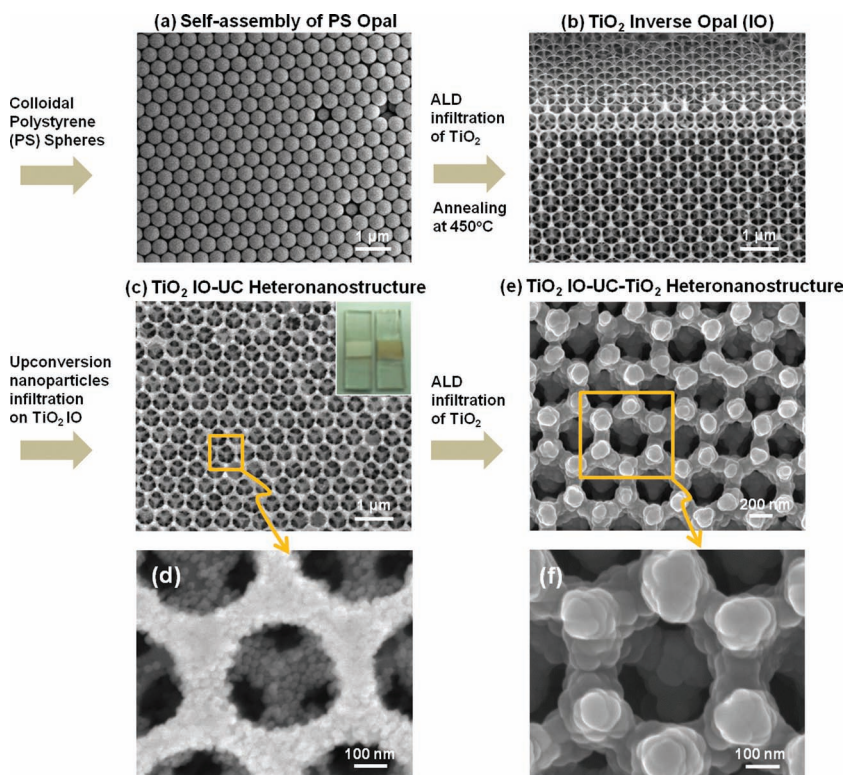


Figure 1. Scanning electron microscopic images showing fabrication process of the three-dimensional hierarchical nanostructured photoanode. a) Self-assembled polystyrene spheres formed on fluorine-doped tin oxide glass. b) TiO_2 inverse opal photonic crystals fabricated by atomic layer deposition. c) Upconversion nanoparticles infiltrated on the TiO_2 inverse opals. (Inset) Photograph of TiO_2 inverse opals (left) and upconversion nanoparticle-coupled TiO_2 inverse opals (right). d) A magnified image of c) showing the nanoparticles on the inverse opal surfaces. e) TiO_2 deposited on upconversion nanoparticles coupled TiO_2 inverse opals. f) A magnified image of e).

dot photosensitizer, which in turn injects electrons into TiO_2 . The whole process of excitation, emission, upconversion, and electron injection is illustrated in **Figure 2**. The visible light emission by nanoparticles and the concurrent absorption by quantum dots in an interconnected porous network present a favorable configuration for the photoanode to exhibit high optical gain, thus increasing the photocurrent in the photoelectrochemical module.

The upconversion luminescence of the nanoparticles was measured before and after the addition of quantum dots to the hetero-nanostructures (**Figure 3**). Without the quantum dots in the photoanode, the intensity of the green emission (522 nm and 540 nm) is higher than that of the red emission (653 nm). In contrast, upon coating of the quantum dots, the green emission is significantly attenuated by more than 50% due to the strong absorption of the quantum dots for charge separation. The spectral absorption of CdSe quantum dots was shown by the diffuse reflectance measurement where the bandgap absorption peak can be noticed at around 540 nm, which matches well with the emission of nanoparticles.

To demonstrate the use of upconversion scheme in a photoelectrochemical module, the electrochemical performance of the hetero-nanostructured photoanode was investigated by

conducting the current vs potential measurements under a dark and 980 nm diode laser excitation at a low power of 500 mW in a three-electrode cell configuration. In addition, the measurements were also carried out for a working electrode which acts as a control group. This electrode consists of titanium oxide inverse opal and CdSe quantum dots, and its fabrication procedures were the same as the one for the hetero-nanostructure but without the infiltration of upconversion nanoparticles. **Figure 4a** shows that the hetero-nanostructured photoanode exhibits a photocurrent of 0.02 mA upon near-infrared laser excitation, indicating an efficient process of conversion of sub-bandgap energy by upconversion nanoparticles to visible light and subsequent absorption by quantum dots for charge separation. Both the current-potential measurement and upconversion photoluminescence measurements verify that the generated photocurrent is attributed to the photon upconversion in the photoelectrochemical cells. The onset potential and the rise of photoresponse with increasing bias voltage are the typical measurements observed for the photoelectrochemical photoanode. **Figure 4b** shows the amperometric (current-time) curve which indicates fast photoresponse and good photostability of the photoanode.

In conclusion, we have demonstrated a new method to utilize upconversion nanoparticles in a hetero-nanostructured photoanode for enhanced near-infrared light harvesting. We show that upconversion is responsible for the observed photoresponse upon near-infrared exposure. This is the first demonstration of photoelectrochemical electrodes with upconversion nanoparticles embedded in porous photonic crystals. The interconnected pores of the photonic crystals render the nanoparticles spatially positioned in close proximity to the CdSe quantum dots, leading to an enhanced energy transfer and light harvesting. This proof-of-concept is highly applicable to other types of solar cells such as thin-film, liquid-junction and organic solar cells where infrared photons with sub-bandgap energies can be harvested for improved photon-to-electricity conversion efficiency by broadening the spectral response.

Experimental Section

Fabrication of TiO_2 inverse opal/upconversion nanoparticle/ TiO_2 hetero-nanostructured photoanode: TiO_2 inverse opal photonic crystals were immersed into a dispersion of upconversion nanoparticles to absorb the nanoparticles onto the TiO_2 internal surfaces. Subsequently, the as-prepared electrode was dipped into deionized water to remove excess nanoparticles on the surface of the inverse opals, and then dried in vacuum. The process was repeated for several times to obtain desired loading of nanoparticles. The electrode was then transferred in an atomic layer deposition reactor for TiO_2 deposition.

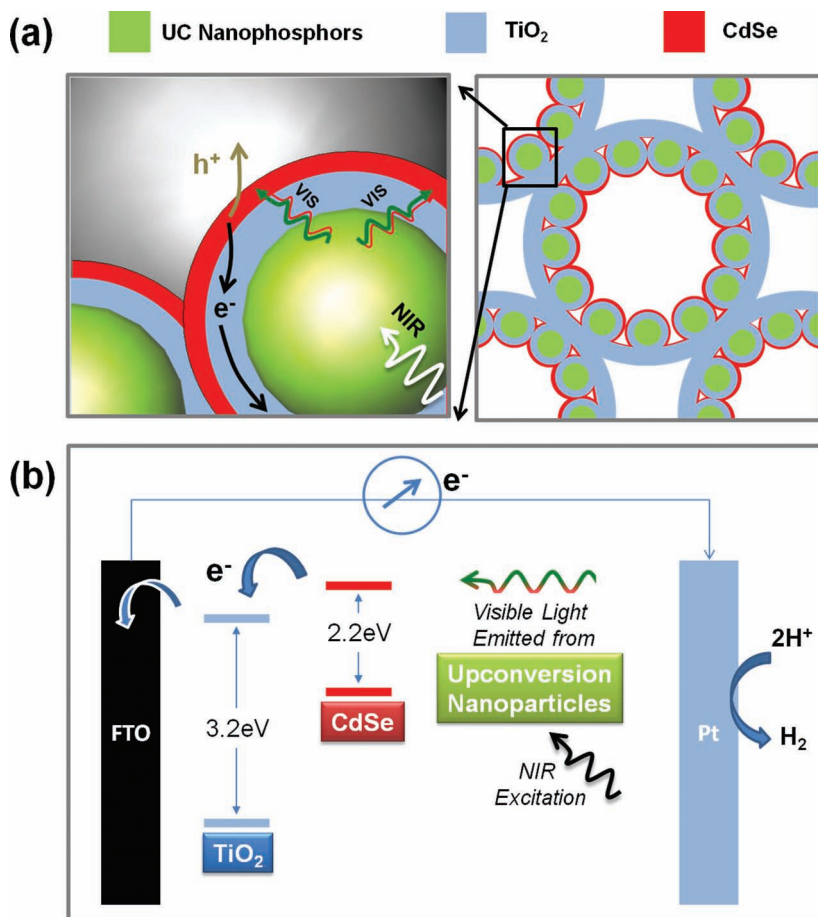


Figure 2. a) Schematic of energy flow in the as-prepared hetero-nanostructures from upconversion nanoparticles to visible light-absorbing CdSe nanoparticles to TiO₂ Inverse Opals upon near-infrared photoexcitation. b) Energy diagram illustrating the charge injection from the excited CdSe into TiO₂ and the transport of photoinjected electrons to the electrode surface for hydrogen generation.

CdSe quantum dot sensitization of hetero-nanostructured photoanode: CdSe quantum dots was the last layer of material deposited on the hetero-nanostructure. The process was carried out by a successive ionic layer adsorption and reaction deposition method.^[15] In a typical procedure, the TiO₂ inverse opals/upconversion nanoparticles/TiO₂ electrode was first immersed into an ethanol solution of cadmium acetate dihydrate (Cd(Ac)₂·2H₂O, 50 mM, Alfa Aesar, 98%) for 1 minute to adsorb Cd²⁺ onto TiO₂ surfaces. It was then rinsed with ethanol to remove excess Cd²⁺ and dried under N₂ gas stream in an argon atmosphere. Subsequently, selenium (Se, Sigma-Aldrich, 99.8%) and sodium borohydride (NaBH₄, Sigma Aldrich, 99.8%) were mixed in water to prepare an aqueous solution containing 50 mM of Se²⁻. The electrode was then dipped into this mixed solution for 1 min, rinsed with ethanol and dried in an argon atmosphere. Here, the Cd²⁺ reacted with Se²⁻ to form semiconductor quantum dots CdSe. The cycle finishes by rinsing of the electrode in ethanol to remove excess ions and drying under N₂ gas in the argon atmosphere. This cycle was repeated for several times to achieve a desirable CdSe loading. Finally, the quantum dots photosensitized electrode was annealed at 300 °C for 30 min in an argon atmosphere to improve the material's crystallinity.

Materials Characterizations: The microstructure of the hetero-nanostructured photoanode was analyzed by using a field-emission scanning electron microscope (JEOL JSM-7600F) and transmission electron microscopes (JEOL JEM 2100F and 1400). The X-ray diffraction pattern of the materials was measured by a Shimadzu thin film diffractometer equipped with Cu-K α radiation. The specular reflectance spectra were collected at 20° with respect to the normal incidence of light using a UV-vis-NIR spectrophotometer (Cary 5000). Upconversion luminescence spectra were measured by exciting samples at 980 nm using a diode laser. The emissions were then collected and dispersed using a monochromator (Princeton Instruments 2300i). The signals were monitored with a thermoelectrically cooled CCD (PIXIS 100).

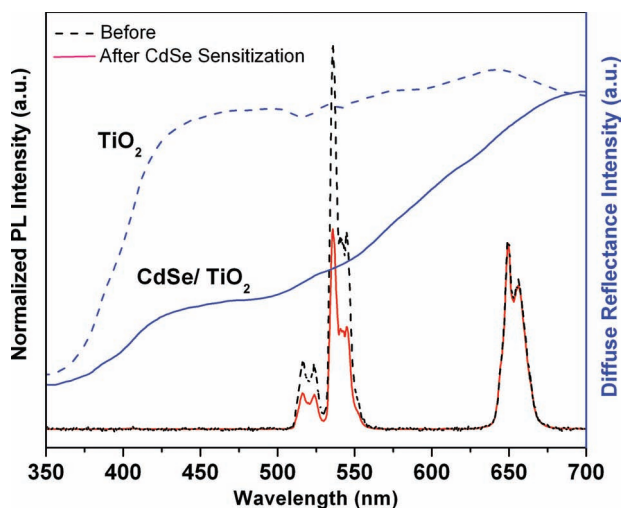


Figure 3. Upconversion emission spectra of upconversion nanoparticles infiltrated TiO₂ inverse opal before and after the coating of CdSe quantum dots. Diffuse reflectance measurement shows the strong visible light absorption of CdSe (dashed and solid lines correspond to data obtained before and after sensitization, respectively).

Supporting Information

Supporting Information is available from the Wiley Online Library or from the author.

Acknowledgements

This study was supported by the Ministry of Education, Singapore (Grant No. T208A1225, AEC 5/08). X.L. acknowledges the National Research Foundation and the Economic Development Board (Singapore-Peking-Oxford Research Enterprise, COY-15-EWI-RCFSA/N197-1) for supporting this work.

Received: October 18, 2012

Revised: November 8, 2012

Published online: January 3, 2013

[1] a) F. Auzel, *Chem. Rev.* **2004**, *104*, 139; b) F. Wang, X. Liu, *Chem. Soc. Rev.* **2009**, *38*, 976; c) M. Haase, H. Schafer, *Angew. Chem. Int. Ed.* **2011**, *50*, 5808; d) A. Kar, A. Patra, *Nanoscale* **2012**, *4*,

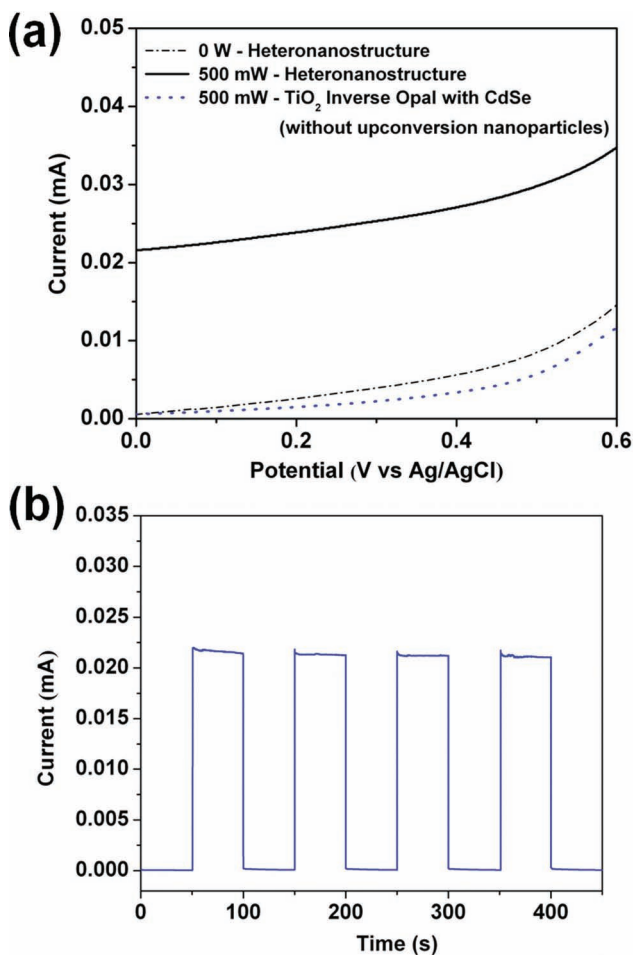


Figure 4. a) Linear sweep voltammetry measurements of the hetero-nanostructured photoanode and a working electrode without upconversion nanoparticles, collected both in the dark and under 980 nm laser diode excitation powered at 500 mW. b) Amperometric curve of the CdSe quantum dot-sensitized hetero-nanostructured photoanode at an applied potential of 0 V versus Ag/AgCl under a laser diode excitation of 980 nm powered at 500 mW with 50 s laser on/off cycles.

- 3608; e) W. Feng, L. Sun, Y. Zhang, C. Yan, *Coordination Chem. Rev.* **2010**, 254, 1038; f) J. Zhou, Z. Liu, F. Li, *Chem. Soc. Rev.* **2012**, 41, 1323; g) F. Wang, Y. Han, C. S. Lim, Y. Lu, J. Wang, J. Xu, H. Chen, C. Zhang, M. Hong, X. Liu, *Nature* **2010**, 463, 1061; h) F. Wang, R. Deng, J. Wang, Q. Wang, Y. Han, H. Zhu, X. Chen, X. Liu, *Nat. Mater.* **2011**, 10, 968; i) G. Lu, S. Li, Z. Guo, O. K. Farha, B. G. Hauser, X. Qi, Y. Wang, X. Wang, S. Han, X. Liu, J. S. DuChene, H. Zhang, Q. C. Zhang, X. Chen, J. Ma, S. C. J. Loo, W. Wei, Y. Yang, J. T. Hupp, F. Huo, *Nat. Chem.* **2012**, 4, 310; j) S. Wu, G. Han, D. J. Milliron, S. Aloni, V. Altoe, D. V. Talapin, B. E. Cohen, P. J. Schuck, *P. Natl. Acad. Sci. USA* **2009**, 106, 10917; k) G. Chen, T. Y. Ohulchanskyy, R. Kumar, H. Agren, P. N. Prasad, *ACS Nano* **2010**, 4, 3163; l) J. Hao, Y. Zhang, X. Wei, *Angew. Chem. Int. Ed.* **2011**, 50, 6876.
- [2] a) H. Wang, M. Batentschuk, A. Osvet, L. Pinna, C. J. Brabec, *Adv. Mater.* **2011**, 23, 2675; b) J. de Wild, A. Meijerink, J. K. Rath,

- W. van Sark, R. E. I. Schropp, *Energy Environ. Sci.* **2011**, 4, 4835; c) P. V. Kamat, *J. Phys. Chem. C* **2007**, 111, 2834; d) P. V. Kamat, K. Tvrđy, D. R. Baker, J. G. Radish, *Chem. Rev.* **2010**, 110, 6664; e) C. Strümpel, M. McCann, G. Beaucarne, V. Arkhipov, A. Slaoui, V. Švrček, C. del Cañizo, I. Tobias, *Sol. Energy Mater. Sol. Cells* **2007**, 91, 238; f) A. Shalav, B. S. Richards, M. A. Green, *Sol. Energy Mater. Sol. Cells* **2007**, 91, 829; X. Huang, S. Han, W. Huang, X. Liu, *Chem. Soc. Rev.* **2013**, 42, 173.
- [3] a) J. Shi, J. Ye, L. Ma, S. Ouyang, D. Jing, L. Guo, *Chem.-Eur. J.* **2012**, 18, 7543; b) Z. Li, F. Shi, T. Zhang, H. Wu, L. Sun, C. Yan, *Chem. Commun.* **2011**, 47, 8109; c) W. P. Qin, D. S. Zhang, D. Zhao, L. L. Wang, K. Z. Zheng, *Chem. Commun.* **2010**, 46, 2304; d) H. Zhang, Y. Li, I. A. Ivanov, Y. Qu, Y. Huang, X. Duan, *Angew. Chem. Int. Ed.* **2010**, 49, 2865; e) S. Schietinger, T. Aichele, H. Q. Wang, T. Nann, O. Benson, *Nano Lett.* **2010**, 10, 134; f) L. Sudheendra, V. Ortalan, S. Dey, N. D. Browning, I. M. Kennedy, *Chem. Mater.* **2011**, 23, 2987; g) W. Zou, C. Visser, J. A. Maduro, M. S. Pshenichnikov, J. C. Hummelen, *Nat. Photonics* **2012**, 6, 560; h) X. Xie, X. Liu, *Nat. Mater.* **2012**, 11, 842; i) M. Saboktakin, X. Ye, S. J. Oh, S. H. Hong, A. T. Fafarman, U. K. Chettiar, N. Engheta, C. B. Murray, C. R. Kagan, *ACS Nano* **2012**, DOI: 10.1021/nr302466r.
- [4] a) A. Shalav, B. S. Richards, T. Trupke, K. W. Krämer, H. U. Güdel, *Appl. Phys. Lett.* **2005**, 86, 013505; b) T. Trupke, M. A. Green, P. Würfel, *J. Appl. Phys.* **2002**, 92, 4117.
- [5] J. de Wild, A. Meijerink, J. K. Rath, W. G. J. H. M. van Sark, R. E. I. Schropp, *Sol. Energy Mater. Sol. Cells* **2010**, 94, 1919.
- [6] a) G. B. Shan, G. P. Demopoulos, *Adv. Mater.* **2010**, 22, 4373; b) C. Yuan, G. Chen, P. N. Prasad, T. Y. Ohulchanskyy, Z. Ning, H. Tian, L. Sun, H. Agren, *J. Mater. Chem.* **2012**, 22, 16709.
- [7] L. Liu, S. K. Karuturi, L. T. Su, A. I. Y. Tok, *Energy Environ. Sci.* **2011**, 4, 209.
- [8] C. Cheng, S. K. Karuturi, L. Liu, J. Liu, H. Li, L. Su, A. I. Y. Tok, H. Fan, *Small* **2012**, 8, 37.
- [9] S. K. Karuturi, C. Cheng, L. Liu, L. Su, H. Fan, A. I. Y. Tok, *Nano Energy* **2012**, 1, 322.
- [10] P. Jiang, J. F. Berton, K. S. Hwang, V. L. Colvin, *Chem. Mater.* **1999**, 11, 2132.
- [11] S. K. Karuturi, L. Liu, L. T. Su, Y. Zhao, H. J. Fan, X. Ge, S. He, A. T. I. Yoong, *J. Phys. Chem. C* **2010**, 114, 14843.
- [12] L. Liu, S. K. Karuturi, L. T. Su, Q. Wang, A. I. Y. Tok, *Electrochem. Commun.* **2011**, 13, 1163.
- [13] a) F. Wang, J. Wang, X. Liu, *Angew. Chem. Int. Ed.* **2010**, 49, 7456; b) G.-S. Yi, G.-M. Chow, *Chem. Mater.* **2006**, 19, 341; c) J. C. Boyer, M. P. Manseau, J. I. Murray, F. van Veggel, *Langmuir* **2010**, 26, 1157; d) R. Deng, X. Xie, M. Vendrell, Y. T. Chang, X. Liu, *J. Am. Chem. Soc.* **2011**, 133, 20168; e) F. Chen, W. Bu, S. Zhang, X. Liu, J. Liu, H. Xing, Q. Xiao, L. Zhou, W. Peng, L. Wang, J. Shi, *Adv. Funct. Mater.* **2011**, 21, 4285; f) Y. Yang, Q. Shao, R. Deng, C. Wang, X. Teng, K. Cheng, Z. Cheng, L. Huang, Z. Liu, X. Liu, B. Xing, *Angew. Chem. Int. Ed.* **2012**, 51, 3125; g) X. Teng, Y. Zhu, W. Wei, S. Wang, J. Huang, R. Naccache, W. Hu, A. I. Y. Tok, Y. Han, Q. Zhang, Q. Fan, W. Huang, J. A. Capobianco, L. Huang, *J. Am. Chem. Soc.* **2012**, 134, 8340; h) F. Vetrone, R. Naccache, V. Mahalingam, C. G. Morgan, J. A. Capobianco, *Adv. Funct. Mater.* **2009**, 19, 2924; i) D. Chen, L. Lei, A. Yang, Z. Wang, Y. Wang, *Chem. Commun.* **2012**, 48, 5898; j) D. Yang, C. Li, G. Li, M. Shang, X. Kang, J. Lin, *J. Mater. Chem.* **2011**, 21, 5923; k) Y. Liu, D. Tu, H. Zhu, R. Li, W. Luo, X. Chen, *Adv. Mater.* **2010**, 22, 3266.
- [14] A. J. L. Sommerdijk, J. Lumin, **1973**, 6, 61.
- [15] D. R. Baker, P. V. Kamat, *Adv. Funct. Mater.* **2009**, 19, 805.